SPECIAL ISSUE ARTICLE

The effects of increasing filler loading on the contact resistivity of interconnects based on silver–epoxied conductive adhesives and silver metallization pastes

Maria Ignacia Devoto Acevedo[1,2] [ORCID] | Rich Wells[3] | Stephan Großer[4] | Karl Wienands[1] | Dominik Rudolph[1] | Andreas Halm[1] | Ralph Gottschalg[2,4] [ORCID] | Daniel Tune[1] [ORCID]

[1]International Solar Energy Research Center (ISC) Konstanz, Constance, Germany

[2]Hochschule Anhalt/Anhalt University of Applied Sciences, Köthen, Germany

[3]Nagase ChemteX America Corp, Delaware, Ohio, USA

[4]Fraunhofer Center for Silicon Photovoltaics (CSP), Halle (Saale), Germany

Correspondence
Maria Ignacia Devoto Acevedo, International Solar Energy Research Center (ISC) Konstanz, Rudolf-Diesel-Straße 15, Constance 78467, Germany.
Email: ignacia.devoto@isc-konstanz.de

Abstract

Our previous work highlighted how microscopic structural effects influence the sheet and contact resistance of electrically conductive adhesives (ECAs). Herein, we delve further by investigating how the contact and bulk resistivity of several ECAs that are based on the same formulation, but with different filler content, are correlated with the filler content. Additionally, two different filler geometries — high and low surface area (HSA and LSA) fillers — are combined in different ratios to maintain a similar viscosity and therefore processability. Hence, contact and bulk resistivities are also correlated with the different geometry ratios of these two fillers. As expected, it was found that the contact and bulk resistivities decreased when the filler content was increased. However, the magnitude of the decrease was found to depend strongly on the filler geometry ratio. At extreme filler geometry ratios, when the bulk is either mostly loaded with HSA-fillers or mostly with LSA-fillers, the impact of changes in the filler content on the bulk and contact resistivities is markedly different. The measured data is interpreted within the context of percolation theory and it is determined that the optimum ratio of the LSA and HSA Ag-fillers investigated in this study is approximately 60:40 (for an epoxy-based adhesive). This work has important ramifications for the design of ECAs, where cost considerations and the need to reduce silver resource usage demand the lowest (silver) filler content, but the demands of product performance point to higher filler content.

KEYWORDS
bulk resistivity, contact resistivity, ECA, ECA–based interconnects, filler content, high surface area fillers, low surface area fillers, TLM

1 | INTRODUCTION

In one of our previous works, it was determined that even when macro-scale inhomogeneities in electrically conductive adhesives (ECAs) (e.g., variations in the thickness) are not present, microscopic structural effects influence the sheet and contact resistance of the ECAs.[1] In particular, variations in the distribution of fillers significantly alter the bulk resistivity of the composites, and this variability is also clearly correlated with differences in the geometry of the fillers.[1] Different models have been developed to explain the conduction mechanisms of ECAs, which are mainly based either on percolation theory[2] or effective media theory.[2] These theories incorporate thermodynamic effects, geometrical differences, and impact on filler orientation and also use statistical tools. The gradual development of models over the years has aimed to construct a single theory that accounts for all (or at least most) of the components of ECAs that affect their electrical conductivity. However, there are a large number of parameters such as filler distribution, shape, size, aspect ratio, and conductivity, as well as the nature of the polymer matrix, interactions between matrix and filler, wettability, viscosity, surface energy, processing technique, etc. This list is by no means complete and with ongoing research and development in conductive adhesives, the list continues to grow. A one-size-fits-all theory has not yet been developed, and it is uncertain whether that is possible at all.

However, it is still possible to further understand the conductive mechanisms of ECAs using a particular theory or model that correctly fits the circumstances of the experiment. In this study, the contact and bulk resistivity of ECAs based on the same formulation, but with different types of filler, is correlated with the amount of filler. By varying the ratio of two different filler geometries, the impact on viscosity and therefore processability due to changing the amount of filler is minimized. Contact and bulk resistivities are also correlated with the different filler geometry ratios between both fillers. The difference between fillers lies in their surface area but their sizes are relatively similar. As will be shown below, percolation theory can be used to estimate a correlation between all the important differences between the conductive adhesives. There is plenty of literature describing conduction theories but these are mostly applied only to bulk resistivity, with the only mention of contact resistance being associated with the constriction resistance, which is the resistance at the contact between two fillers. However, to the best of our knowledge, none of these theories has been used to try to understand contact resistivity at an application level. Furthermore, many of them deal with nanocomposites because the filler geometry of nanotubes, nanowires, carbon black, etc., tends to be extreme.

This work aims to expand on these unexplored areas by studying the impact of the increase in filler content and changes in the filler geometry ratio on the bulk resistivity of an epoxy-based conductive adhesive as well as on the contact resistivity between the adhesive and the metallization paste used on silicon solar cells. To conduct this research, two different filler geometries are used to control the viscosity of the adhesive formulation when the total filler content is varied. These fillers are not extremely dissimilar nor do they possess extreme geometries when compared to each other. The fillers are in the micrometer range; they are not nanoparticles. Moreover, both fillers

are made of silver so the conductivity of the epoxy polymer is practically negligible in comparison. Considering these conditions and comparing the different theoretical models used to describe conduction in bimodal composites, as given in the following section, it is possible to determine an optimal filler geometry ratio using percolation theory. More precisely, this study aims to answer the following questions:

a. how is the contact and bulk resistivity impacted when increasing the total filler content?
b. what are the effects on the contact and bulk resistivity when the ratio between two different fillers changes?
c. what is the optimal filler geometry ratio given these two different filler geometries?

To answer these questions, several samples with different amounts of filler content and different filler geometry ratios are manufactured and their contact and bulk resistivities are measured. Results are analyzed straightforwardly by direct comparison with filler content and filler geometry ratio. Ultimately, the aim of this work is to be able to produce ECAs with the lowest silver content while also minimizing the bulk and contact resistivities.

2 | BIMODAL COMPOSITE CONDUCTIVITY MODELS

Unfilled and uncured epoxy, acrylate, and silicone polymers have a resistivity in the range of 10^{12}–10^{15} Ω cm.[3] To manufacture ECAs, polymeric resins are filled with a *critical volume fraction (percolation threshold)* of conductive fillers that, after curing, becomes conductive (10^{-3} – 10^{-4} Ω cm).[3] At first, mixture rules and later *effective media theories* (EMTs) were used to analyze the data from conductor-insulator composites. However, since the 1970s, due to the realization that the percolation threshold in such systems is a critical point of transition, the main theoretical models have involved *percolation theory* (PCT) and the concept of *scaling*.[4] Scaling laws have the form $Q \propto |\Phi - \Phi_c|^t$, where Q is the physical property, such as electrical conductivity, t the *exponent*, Φ the volume fraction of the conductive phase, and Φ_c its critical volume fraction.[4] The most important distinction between percolation theory (and scaling laws) and effective media theory resides in the conditions in which these theories can be applied or used. PCT is mostly reliable when the ratio of the conductivities of the two phases is small, i.e., when their conductivities are very dissimilar; whereas EMT is better applied to cases where phases have comparable conductivities.[4] Additionally, EMT works best at lower values of volume fraction, as one phase, modeled as a sphere or ellipsoid, is surrounded by a mixture of the two phases that has the mean or effective value of the medium.[2] In contrast, PCT, which is limited in its applicability to the matrix sites occupied by spherical particles, predicts that the resistivity of the overall composite depends only on the volumetric concentration of the phases. However, care must be taken when using PTC, as research on nanocomposites has already shown that microscopic effects play a major role in the physics behind the conductivity of bimodal composites.[5–8]

According to a review of electrical conductivity models for conductive polymer composites, due to the influence of different parameters, as mentioned above, there are four main classes of conductivity models: statistical, thermodynamic, geometric, and structure-oriented models.[6,8,9] Different models found in the literature are classified into these four main categories and shortly described in the list below.

- **Statistical percolation models**: Most conductivity models found in the literature are of the statistical percolation type. They typically predict the conductivity assuming a volume fraction as a base and then calculating the probability of particle coming into direct contact within the composites.[6,8] Computer simulations are normally used to predict the points and bonds that are formed in a cluster and to determine how many of those clusters percolate across the whole adhesive bond width. Although these types of models are not completely accurate due to the absence of microscopic effects, they have become the basis for many later conductivity models.[6,8] Particularly important is the general effective medium theory developed by McLachlan, which combines percolation and effective medium theories to overcome several limitations of each theory.[10,11]

- **Thermodynamic models**: These are considered to be thermodynamic models because they consider factors such as filler and polymer surface energies and polymer melt viscosity, among others. A model developed by Mamunya et al[12] showed that percolation behavior was dependent on the polymer filler interaction, in addition to the size and amount of the filler material. Although this model was found to be the one that better agreed with experimental data, it was also found to be limited by the surface energy input values, where high values cause a breakdown in the system equations.[6]

- **Geometrical percolation models:** These were initially intended to predict the conductivity of sintered mixtures of conducting and insulating powders. A well-known model proposed by Malliaris and Turner[13] uses the diameters of particles, the probability for the occurrence of long bands of particles, and the arrangement of the conductive particles on the surface of the insulating particles. However, the model did not accurately predict percolating volume fractions when compared to experimental data.[6]

- **Structure-oriented percolation models**: These are based on the physical construction of the final composite, which depends on filler morphology and adhesive processing techniques. The Nielsen model related the conductivity of a composite to the aspect ratio and the coordination of the filler, but Bigg found it to be ineffective in predicting the electrical conductivity.[6,14,15] Additionally, Weber and Kamal[16] proposed two models considering filler concentration, dimensions, aspect ratio, and orientation. However, even if some of these models can accurately predict conductivity, they do not account for surface energy interactions, which are shown to be very important.[6]

The PCT yields phenomenological equations that cannot be derived by first principles. Although the theory was developed in the context of regular lattices, it can also be used to explain continuum systems, such as ECAs, i.e., systems with irregular particle arrangements with an average size in the micrometer range. As shown in Figure 1, PCT considers a lattice that is built up of empty sites (white circles) that are filled (black circles) with a random probability Φ, where bonds (lines) are formed between direct neighboring sites. Finite isolated clusters start forming up to a critical volume fraction, Φ_c, where a percolating cluster is able to conduct current between two opposite electrodes. For $\Phi < \Phi_c$ the composite acts as an insulator, while at $\Phi \sim \Phi_c$ there is an *insulator-conductor transition* and a finite conduction is established. Above Φ_c the effective conductivity of the composite (σ_m) is found to increase as $\sigma_m = (\Phi - \Phi_c)^t$, where t, called the universal exponent, is usually in the range of 1.65–2.0 for three-dimensional systems.[11]

Calculating the conductivity caused by continuous percolation clusters above and around Φ_c requires a knowledge of the internal structure of large clusters. Non-percolating (or finite) clusters do not contribute to the overall conduction while dangling bonds only contribute to the percolation cluster density but not to its conductivity. Hence, in reality, the conductivity is neither proportional to Φ nor to Φ_c.[5] When all dangling bonds are removed, only the backbone is left for conduction. The removal of any single bond from the backbone will break the interconnection path across the electrodes, while the removal of one multi-bond will still allow the flow of the current through another parallel path. In reality, the current flows through a fraction of the sample which is significantly less than Φ_c. In practice, only volume fractions greater than 25–35% of Ag flakes are of real interest in commercial epoxy-based ECAs.

The percolation equations for the conductivity of a bimodal composite (i.e., with a highly conductive phase and a poorly conductive phase) such as an ECA are given in three distinct regimes[2,11]:

$$\sigma_m \approx \begin{cases} \sigma_h(\phi - \phi_c)^t & \text{where } \phi > \phi_c & \text{Conductive regime} \\ \sigma_l(\phi - \phi_c)^{-s} & \text{where } \phi < \phi_c & \text{Insulating regime} \\ \sigma_l^u \sigma_h^{1-u} & \text{where } |\phi - \phi_c| = \delta & \text{Critical region} \end{cases}$$

where σ_m is the conductivity of the composite, Φ and σ_h are the volume fraction and the conductivity of the highly conductive phase; σ_l is
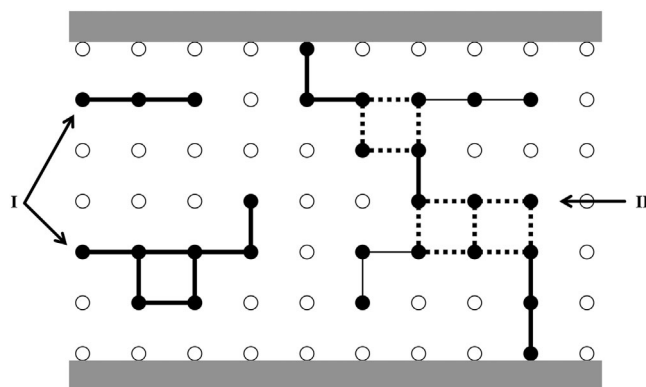

FIGURE 1 Example of clusters and types of interconnections for PCT, where **I** denotes small (finite) clusters and **II** denotes percolation (infinite) clusters. Thick continuous lines represent "single-bonds" while thick dashed lines are "multi-bonds". Thin continuous lines denote "dangling-bonds".

the conductivity of the poorly conductive phase; Φ_c is the percolation threshold; and $u = t/(t + s)$, where s and t are exponents, which were believed to depend on whether the system was two dimensional (such as a film or an anisotropic adhesive) or three dimensional (such as the bulk of an isotropic adhesive). The width of the critical region δ in DC (or very low frequency) is given by $\delta = (\sigma_l/\sigma_h)^{1/(t + s)}$. In the conductive region, many conductive paths exist across the sample and if $\sigma_h >> \sigma_l$, then the insulating phase has no effect on first order. When σ_h/σ_l is not zero, it is necessary to consider this critical region, near Φ_c, where the system moves from the insulating to the conductive regime as Φ increases. However, the expression for σ_m is constant in the critical region, which is not the case in practice. According to measurements of the percolation threshold, the data may be fitted with what is called the normalized percolation equations[2]:

$$
\sigma_m = \begin{cases} \sigma_h \cdot \left(\dfrac{\phi - \phi_c}{1 - \phi_c} \right)^t & \text{where } \phi > \phi_c \\[3mm] \sigma_l \cdot \left(\dfrac{\phi_c - \phi}{\phi_c} \right)^{-s} & \text{where } \phi < \phi_c \end{cases}
$$

Until the 1990s it was believed that the exponents s and t only depended on the dimension of the problem and the most widely accepted universal values for three-dimensional problems were $s \approx 0.76$–0.89 and $t \approx 1.7$–2.0.[2,17–19] However, since then, non-universal exponents have been observed and predicted.[2,4,11,20–23] Experimental data show that a proper model for the conductivity of composites using conducting fillers that possess extreme geometries, such as nanotubes, nanowires, and graphite, among others, can only be achieved with non-universal exponents.[11] It is hypothesized that non-universal values are probably due to extensive quantum mechanical tunneling and that the universal exponent indicates classical (non-tunneling) systems that have fairly uniform structures.[2] Moreover, PCT assumes only metallic conduction between particles in direct contact and does not consider the finite resistance of tunneling conduction across the insulating gaps or constriction resistance caused by the small contact area between the particles.[7] It is argued that tunneling must be accounted for in non-universal values of t and s.[24,25] As filler geometry plays an important role in the conduction behavior of ECAs, two fillers with different geometries are used to explore their impact on bulk and contact resistivity.

It is important to consider that constriction and tunneling resistances depend on microscopic effects and that depending on the filler geometries, one or the other resistance can dominate the conductive behavior of the paste. Microscopic effects include filler size, distribution and orientation; and even pressure between fillers; decomposition of organic insulating coating at high temperatures; broken contacts; changes in the interconnection due to coefficient of thermal expansion (CTE) mismatch during temperature changes, etc.[5,7] The contacting spot area between flakes is affected by the presence of insulating coatings on the flakes, thus, only a fraction of the contacting spot acts as a *metallic contact* while another fraction acts as a *quasi-metallic contact*.[5] Such insulating coatings prompting tunneling effects can be composed of residual organic and tarnish films, or thin epoxy layers.[7] Quasi-metallic contacts are only penetrable by electrons by means of tunneling, for which the potential barrier is proportional to the work function of the conductive filler and of the thin film, where the film can be the insulating material or coating or any residual film). Pressure applied during curing of the adhesive or generated in later thermal cycles enlarges the metallic contact area by elastic and plastic deformation producing fresh metallic contacts and thus decreasing the resistivity of the adhesive.[5] Moreover, percolation clusters already exist in the matrix before the cure process takes place and the sudden conduction development is mainly caused by the residual stress and epoxy cure shrinkage contributing to one or more linkages in the percolating backbone paths.[5] This theory has been found to work when composites are made with phases of dissimilar conductivities using fillers without extreme geometries.

3 | EXPERIMENTAL DESIGN

3.1 | Conductive adhesives under investigation

Ten different conductive adhesives were prepared with the same chemical composition using an epoxy polymer filled with silver particles. The filler content was increased in each subsequent group from 60 wt% up to 84 wt% (see Table 1). However, the enlarged number of fillers within the adhesive inherently increases the viscosity of the paste, which eventually reaches a threshold value at which it cannot

Group	Filler geometry ratio	Filler content (wt%)	Filler content (vol%)
G00/Ref	Very high SA	60	13.5
G01	High SA	60	13.5
G02		65	16.1
G03		70	19.6
G04	Medium SA	70	19.6
G05		74	22.9
G06		78	27.0
G07	Low SA	78	27.0
G08		81	30.8
G09		84	35.4

TABLE 1 ECA filler content in wt% and calculated in vol% for the 10 groups studied. The groups are distributed in four different ratios of high and low surface area particles.

be processed in the application. To maintain processability, the thixotropy was controlled using two different filler geometries combined in varying ratios. One filler has a high surface area (HSA) to volume ratio, with an average particle size of 5 μm and average thickness of 0.5 μm; the other filler has a low surface area (LSA) to volume ratio, with an average particle size of 6 μm and average thickness of 2 μm (see Figure 2). This means that in a unit of volume packed with HSA-fillers, there is a higher total amount of surface-to-polymer interaction when compared with the same unit of volume packed with LSA-fillers. Hence, low (high) surface area (to volume ratio) filler promotes lower (higher) viscosities.

As shown in Table 1, four different filler geometry ratios were used in this experiment. These ratios are specified in Table 2. The group G00 uses a *very high SA* ratio that contains 100% of the HSA-filler and is considered to be the reference group. Groups G01 – G03 use a conductive adhesive with *high SA* ratio (35:65), groups G04 – G06 with *medium SA* ratio (69:31), and groups G07 – G09 with *low SA* ratio (94:6). Hence, the total filler content is gradually increased while the filler geometry ratio is maintained constant. Once a threshold in the viscosity is reached, the bulk of the adhesive is disrupted by increasing the percentage of LSA-fillers and reducing the percentage of HSA-fillers in the mixture. Once again, the total filler content is further increased at a constant filler geometry ratio up to a second threshold and then more LSA-fillers are added while HSA-fillers are reduced. Groups G00/G01, G03/G04, and G06/G07 act as further
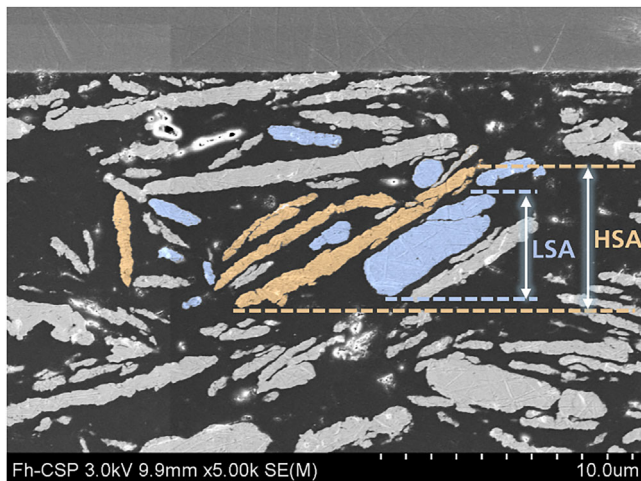
controls to investigate the effect of the change of the filler geometry ratio at a constant filler content.

Very high SA, *high SA*, *medium SA*, and *low SA* are qualitative filler geometry ratios that indicate a range from high to low amounts of HSA-fillers within the different adhesives under study. These qualitative ratios help the reader to easily follow the author's thinking process to understand the results and discussions presented in this work. However, a quantitative representation of these ratios is necessary for plotting important relationships among the bulk and contact resistivity and amount of filler content. Hence, the same ratios are represented by *r* quantitatively, where *r* is defined as the percentage of LSA-fillers over the percentage of HSA-fillers. Therefore, the lowest value of *r* is 0 in the absence of LSA-fillers (*very high SA*) and its highest value is 15.67 when the percentage LSA-fillers is maximized (*low SA*).

3.2 | Test structures and sample characterization

3.2.1 | Viscosity and thixotropy of conductive adhesive

During dispensing, adhesives require low-viscosity behavior in order to flow and create the desired dispensing pattern onto a particular surface. Hence, directly after dispensing, adhesives must retain such a pattern. For that, the paste must display or go back to a high-viscosity behavior so slumping is avoided. By using rheology modifiers and in the absence of shear forces, ECAs form a 3D network structure, due to strong interparticle attractive forces. This network causes a large increase in the viscosity at rest. When applying shear forces, i.e., when the adhesive is dispensed, this network is broken down resulting in dispersed aggregates. As the network breaks down, the viscosity decreases dramatically in what is termed *shear thinning*. Once the shear forces are removed, i.e., when the pattern is placed over a surface, at rest, aggregates can re-form the 3D network.

Although *shear thinning* is a very important part of the dispensing performance for ECAs, most (if not all) technical data sheet for ECAs indicates what is known as the *thixotropic index* or *thixotropy*. This index is defined as the viscosity at a certain shear rate over the viscosity at a shear rate that is 10 times larger. This means that the *thixotropy* is measured over a relatively limited shear rate range. As this range is so limited, this *index* cannot really measure *thixotropy*. The *thixotropic index* is really a measure of the *shear thinning index* since the former relates to how fast the viscosity is changing in the

FIGURE 2 Geometry comparison between HSA-filler (orange) and LSA-filler (blue).

TABLE 2 Percentage ([†]) of HSA and LSA filler for the four filler geometry ratios used in this study.

Filler geometry ratio	HSA content (%)	LSA content (%)	r
Very high SA	100	0	0
High SA	65	35	0.54
Medium SA	31	69	2.23
Low SA	6	94	15.67

[†]As both types of filler are made of silver, they have the same density. Therefore, the content of LSA-fillers and HSA-fillers can be determined in either wt% or vol%. No matter which one is used (wt% or vol%) the percentage and the ratio will remain the same.

dispensing region. If the adhesive were Newtonian, its *thixotropic index* would be near 1 and the dispensed adhesive could be easily pulled by capillary forces and surface tension. However, if the dispensed adhesive had a yield point greater than the capillary forces, its *thixotropic index* would be greater than 1 and it may not flow over the surface. For many commercially available ECAs, the *thixotropic index* ranges from 3 to 6, which allows the adhesive to not slump or sag after dispensing.

Joshi et al rheological behavior during a transient of a wide range of materials presented an assessment of various criteria proposed in the literature for commonly known non-thixotropic viscoelastic materials –polymeric liquids.[26] They indicated that the proposed criteria in the literature do not successfully distinguish thixotropic behavior and intrinsic viscoelastic behavior (including non-linear viscoelasticity such as shear thinning). Hence, up to this day, there is no universal agreement on a clear demarcation between both behaviors. Therefore, this work uses the thixotropic index because it is used by manufacturers of ECAs in their data sheets. However, this index is indeed referring to *shear thinning* behavior and must not be confused with the thixotropic behavior investigated in rheological tests such as the hysteresis-loop test and/or steady shear rate test and similar tests applied to understand rheological changes of ECAs, such as the results presented by Durairaj, Ekere, and Salam in Ref.[27]

In this work, the viscosity of each conductive adhesive was measured using a Brookfield DVNext rheometer at 0.5 rpm (1.9 s^{-1}) and 5.0 rpm (19 s^{-1}). The test was performed at a temperature of 25°C using a cone plate gap of 5·10^{-4} in. (12.7 μm). The thixotropy was calculated as the viscosity at 0.5 rpm over the viscosity at 5.0 rpm.

3.2.2 | Microstructure of conductive adhesive

The determination of the ECA microstructure is required to reveal the existing ECA composition (volume and interface) and exclude potential impacts of interface d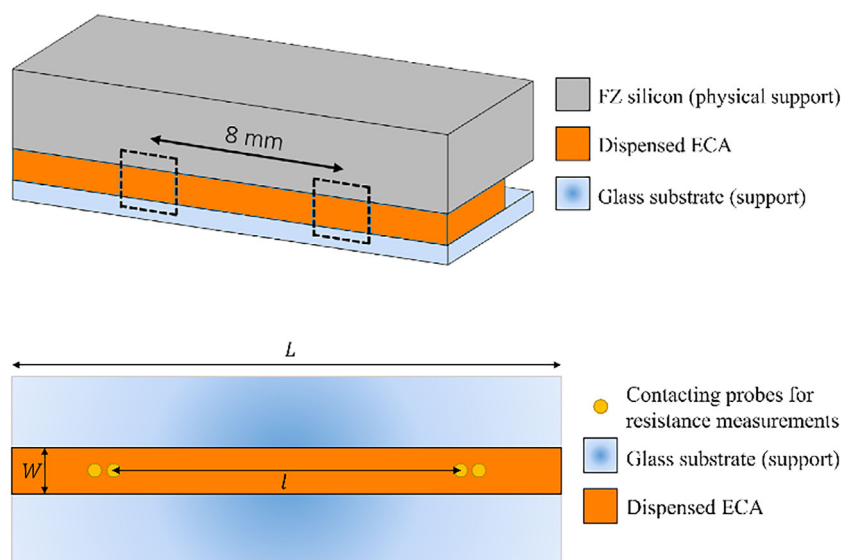elamination, cavities, or filler segregation. A flat interface between ECA and silicon was realized on flat samples designated for the microstructure analysis. On polished 12.4 cm float-zone (Fz) silicon wafers, continuous ECA lines were jet-dispensed and afterward covered with a thin microscope cover glass. The curing of the adhesive was performed in a membrane-type industrial photovoltaic module laminator at 180°C over 10 min while applying a membrane pressure of 1.0 bar with the module chamber at 0 bar, relative to the atmosphere. Afterward, the samples were left to cool to room temperature.

From each test sample, a cm-long segment from the ECA line center was gently separated after laser cutting to avoid preparation artifacts at the silicon–ECA interface. Afterward, each segment was fixed by embedding in a resin. Mechanical grinding and polishing were used to expose the cross-section. The cross-section was centered and aligned parallel along the ECA line. To avoid the charging of insulating materials in scanning electron microscopy (SEM), the samples were coated with conductive carbon. SEM was performed on an FE-SEM HITACHI SU-70 at 3 keV acceleration voltage and different magnifications. On each cross-section, two areas separated by a distance of 8 mm were investigated (see Figure 3). The positions represent equivalents to the distance between most inner contacts in the contact resistivity test structure (see **section 3.2.4**).

3.2.3 | Volume resistivity of conductive adhesive

Dedicated test structures (see Figure 4) were manufactured to determine the volume resistivity of the bulk for each adhesive. Each adhesive composition was dispensed on a glass slide filling a rectangular cavity with a nominal width and length of 0.25 in. ($W = 0.64$ cm) and 3 in. ($L = 7.62$ cm), respectively. The cavity was filled with enough adhesive and the residual material was scraped off. Afterward, three samples per group were cured at 150°C over 1 h on a forced hot air oven and were left to cool to room temperature. Several 4-point measurements were performed on top of the sample at a distance of 2 in.

FIGURE 3 Schematic of the flat cross-section sample design for ECA microstructure analysis that represents two contact positions of the contact resistivity test structure. Not to scale.

FIGURE 4 Dedicated test structure to determine the bulk resistivity of a conductive adhesive. Four-point measurement scheme is shown by the four yellow probes.

($l = 5.08$ cm) using a Keithley 2,750 digital multimeter (see yellow probes in Figure 4). The height of the adhesive was calculated as the average height measured by a drop gauge, where the resistance readings were made including an extra measurement at the middle of the device. The actual width of the adhesive was measured using a caliper at the same positions that the height was measured and an average was determined. The bulk resistivity, ρ, was subsequently determined using **Equation (1)**:

$$\rho = \frac{1}{3} \sum_{i=1}^{3} \frac{R_i W_i t_i}{l} \tag{1}$$

where the index i corresponds to the ith sample; R (in Ω) is the total measured resistance for an adhesive bulk with a length of l (in cm); and W and t (in cm) are the average width and the height/thickness of the adhesive. According to measurements, the average height of the adhesive (in Figure 4) for all samples is 30 μm.

3.2.4 | Contact resistivity of metallization–adhesive interface

As determined in previous work,[28] the test structure used to determine the contact resistivity of ECA-based bonds is shown in Figure 5. Crystalline Czochralski (Cz) n-type wafers were etched around 5 μm per side with NaOH to remove the saw damage and afterwards cleaned (HCl/HF) using a wet-bench. A SiN_x layer was deposited using a PECVD furnace. The metallization was done via screen printing using a non-fire-through paste. The paste was dried in a belt furnace and sintered in a fast-firing belt furnace at around 800°C. As the paste is non-fire-through and the passivation layer is not opened, the silicon bulk is not in direct contact with the metallization (fingers). Therefore, the wafer (including all layers) is only meant for physical support for the metallization. The nominal finger width, L, is 150 μm and corresponds to the screen opening for the fingers. The distance between consecutive fingers (center to center), Δ, is fixed and equal to 6, 8, and 10 mm from left to right and W is the width of the ECA line.

The adhesive was automatically jet-dispensed by a robot, where dispensing parameters (e.g., temperature, speed, pressure, and opening/closing times of the tappet, etc.) were experimentally determined for each adhesive. After dispensing the adhesive, a thin microscope cover glass (0.15–0.16 mm) was placed on top of the whole ECA line without applying any pressure. The curing of the adhesive was performed in a membrane-type industrial photovoltaic module laminator at 180°C over 10 min applying a membrane pressure of 1.0 bar with the module chamber at 0 bar relative to atmosphere. Afterward, the samples were left to cool to room temperature.

As samples are manufactured by dispensing a line perpendicular to the metal fingers (see Figure 5) and the filler content within the adhesive of different groups is increased, samples from different groups are comparable only if they possess the same volume of adhesive. Hence, samples from group G00 are manufactured first by tunning the speed, pressure, temperature, and opening and closing valve times during dispensing to achieve a homogeneous straight line. Afterwards, the amount of ECA to be dispensed on samples from groups G01 – G09 is determined according to the density of each paste. As shown in Table 3, the density of the reference adhesive is 2.37 g cc^{-1}, thus, a 48 mm dispensed line with an average weight of 2.43 mg means a targeted volume per millimeter of adhesive of $2.14 \cdot 10^{-5}$ cc mm^{-1} for G01 – G09. As all samples are manufactured with a 48 mm ECA line, the targeted weight for each group is determined as:

$$m_{GXX} = V_{G00} \cdot \rho_{GXX} \tag{2}$$

where m_{GXX} is the targeted weight of ECA for samples of group GXX, ρ_{GXX} is the density of the ECA for samples of group GXX and V_{G00} is the average volume of the whole ECA line for samples of group G00. ρ_{GXX} is calculated using the reported density values of each raw material. The third column in Table 3 shows the targeted weight of ECA (in mg) for each group while the last column shows the actual average weight (in mg) measured after dispensing the adhesive during the manufacture of the samples.

To determine the contact resistivity for each single sample, a validated method based on the end-contact TLM model was used, where TLM stands for transmission line method (or transfer length method).[28] Figure 6 shows a general equivalent electrical circuit of the test structure shown in Figure 5, which considers three arbitrary contacts (i, j, and k). R'_m and R''_m (Ω) refers to part of the total resistance of the finger; R_f (Ω) is the front-contact resistance; R_e (Ω) is the
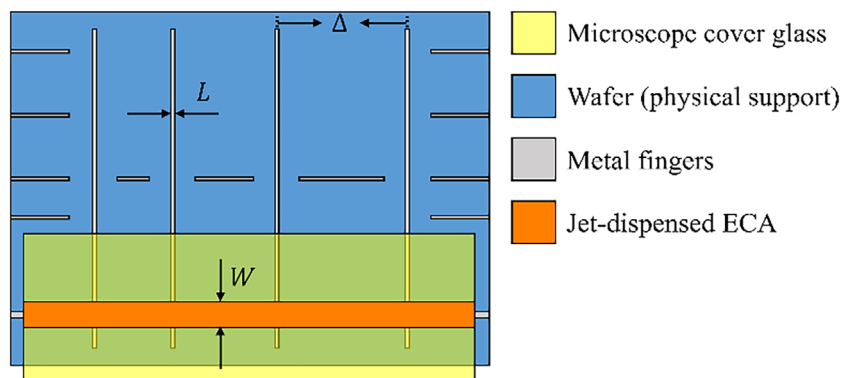

FIGURE 5 Schematic of the test structure used to determine contact resistivity.

Group	Density (g cc⁻¹)	Targeted ECA weight (mg)	Measured ECA weight (mg)
G00 (Ref)	2.37	--	2.43
G01	2.37	2.43	2.53
G02	2.61	2.68	2.63
G03	2.93	3.01	2.96
G04	2.93	3.01	2.98
G05	3.24	3.33	3.42
G06	3.63	3.73	3.68
G07	3.63	3.73	3.73
G08	3.99	4.10	4.00
G09	4.42	4.55	5.05

TABLE 3 Calculated density for each ECA group and their respective targeted and measured weight of ECA for a 48 mm adhesive line.
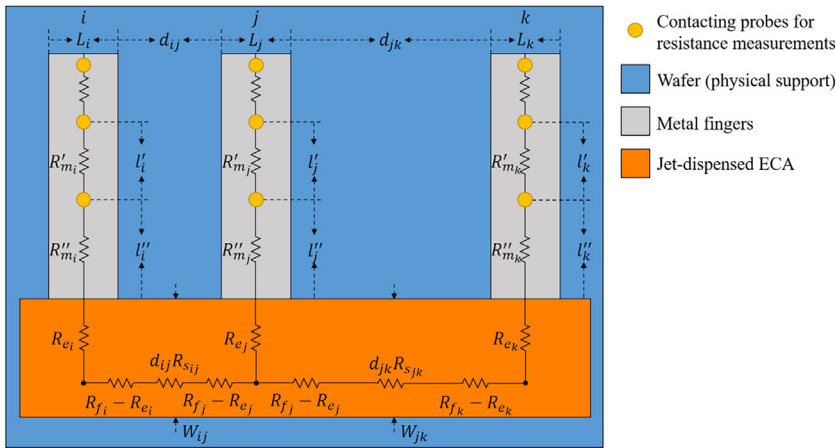

FIGURE 6 General equivalent circuit of the test structure used to determine the contact resistivity of ECA–based bonds.

end-contact resistance; d (mm) is the distance from edge to edge between fingers; R_s (Ω mm⁻¹) is the sheet resistance of the ECA per unit width; l' and l'' (mm) are lengths of fingers and W (mm) is the width of the ECA line. The yellow circles represent the pins of the measuring equipment. The distance between the pins contacting the same finger is 5 mm.

To determine the contact resistivity of a sample, ρ_c (Ω m²), the contact resistivity of the two inner contacts, ρ_{cj}, is first determined. The average between both of them corresponds to the contact resistivity at the sample level. ρ_{cj} is calculated using the end-contact TLM model. The set of equations required to determine all necessary parameters are presented by **Equation (3)–(10)**[28]:

$$R_{e_j} = R_{s_j} \cdot L_{t_j} \cdot \sinh^{-1}\left(\frac{L_j}{L_{t_j}}\right) \tag{3}$$

$$\rho_{c_j} = R_{s_j} \cdot W_j \cdot L_{t_j}^2 \tag{4}$$

$$\rho_c = \frac{1}{N-2} \sum_{j=2}^{N-1} \rho_{c_j} \tag{5}$$

where L_j and W_j are determined as:

$$L_j = \frac{L_i + L_j + L_k}{3} \tag{6}$$

$$W_j = \frac{W_{ij} + W_{jk}}{2} \tag{7}$$

while R_{ej} and R_{sj} are determined as:

$$R_{s_j} = m_j \tag{8}$$

$$R_{e_j} = \frac{V_{jk}}{I_{ij}} - r_j \cdot l_j'' \tag{9}$$

where m_j is the slope of the fitting for the resistance–distance curve using contacts i, j, and k and r_j is the line resistance for the jth finger determined as:

$$r_j = \frac{V_j}{I_{jk}} = \frac{R'_{m_j}}{l_j'} \tag{10}$$

For more details on how to use **Equation (3)–(10)** and the measurements involved in the procedure, please refer to Ref.[28]

Electrical measurements were executed in a single contacting event using three rows of four (12 in total) flat–headed pins with a contacting diameter of 1.5 mm. During any measurement, a DC current (*I*) was injected while a DC voltage (*V*) was measured using a Keithley 2602A source meter. A multiplexer with 72 channels was used to control the function of each probe, i.e., high source, high sense, low source, and low sense, in a 4-point measurement. To prove that the measurement was done in an ohmic operating range, a current sweep was performed (0.01–0.05 A) and the linearity of the current–voltage characteristic was checked via the *Pearson coefficient*. To increase accuracy, the current was first injected in one direction followed by a second measurement in which the current flowed in the opposite direction. The average between both measurements was used for further calculations.

Optical measurements were taken with a Micro-Vu light microscope so as to accurately determine the physical contact area, which is defined by the effective area of metallic surface wetted by ECA. More precisely, the width of the finger (contact length) and the width of the ECA dispensed over the finger (contact width).

4 | EFFECTS OF INCREASING FILLER LOADING/CONTENT

4.1 | Viscosity and thixotropy of ECAs

Figure 7 shows the measured viscosity at 0.5 rpm (○) and 5.0 rpm (+) and includes the results of the calculated thixotropy (●) for all groups, where each color represents a different filler geometry ratio according to Table 2. The reference group has a viscosity of 48,050 mPa s at 0.5 rpm and of 9,610 mPa s at 5.0 rpm, leading to a thixotropy of 5.00. When the total filler content is increased, the thixotropy tends to slowly increase and then rapidly decrease. To avoid further
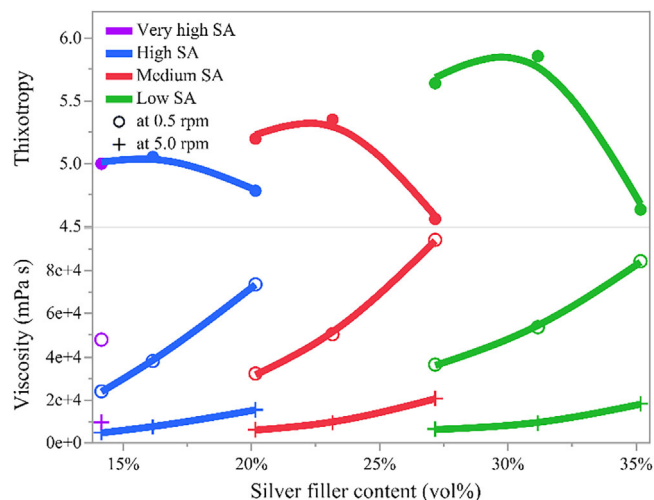
decrease of the index, the filler geometry ratio changes to *medium SA* and the thixotropy increases again. The same happens when changing to a *low SA* filler geometry ratio, however, the thixotropy decreases even faster for formulations with a higher content of LSA-fillers. Nevertheless, the thixotropy slightly varied from the targeted value of 5.00, displaying a minimum value of 4.56 up to a maximum value of 5.86 with an average of 5.11. This allowed the manufacture of samples from all groups without having any processing issues and the targeted amount of paste for each group was easily achieved (see Table 3).

It is interesting to highlight that changing the filler geometry ratio at a constant filler content has an important impact in the performance of the adhesive. Figure 7 shows that at a constant filler content (i.e., at 19 vol% and 27 vol%) the viscosity always decreases when the bulk of the adhesive is disrupted with more LSA-fillers (blue to red and red to green transitions). At the same time, the thixotropy always increases with more LSA-fillers, because the decrease in viscosity is more severe at higher speeds (5.0 rpm). As it will be shown in the next sections of this study, the effects of different filler geometry ratios not only impact the physical parameters of the adhesives but also their electrical performance.

4.2 | Volume resistivity of ECAs

Figure 8 shows the bulk resistivity when the filler content is increased, where the lines are only meant as a guide for the eyes and do not have any physical meaning nor represent any fit. According to the log–plot, the bulk resistivity decreases with the increase in the filler content, as expected. Depending on the filler geometry ratio, the impact on the reduction of the bulk resistivity is different (see fourth column in Table 4). When the bulk contains a larger amount of HSA-fillers (blue line), the initial increase in filler content (5.0 wt%, approx. 3 vol%) reduces the volume resistivity by 70% relative to its initial
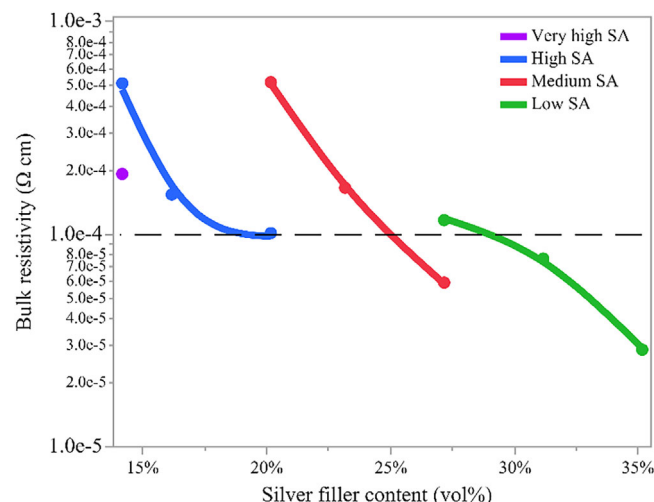

FIGURE 7 Measured viscosity (in mPa s) at 0.5 rpm and at 5.0 rpm and calculated thixotropy for increasing total silver filler content (in vol%).

FIGURE 8 Measured volume (or bulk) resistivity (in Ω cm) for increasing total silver filler content (in vol%).

Group	Filler geometry ratio	Bulk resistivity (Ω cm)	$|\Delta\%_{rel}|$	
G00	Very high SA	$1.92 \cdot 10^{-4}$	--	Initial value
G01	High SA	$5.14 \cdot 10^{-4}$	Initial value	167
G02		$1.54 \cdot 10^{-4}$	70	--
G03		$1.01 \cdot 10^{-4}$	34	Initial value
G04	Medium SA	$5.20 \cdot 10^{-4}$	Initial value	44
G05		$1.65 \cdot 10^{-4}$	68	--
G06		$5.93 \cdot 10^{-5}$	64	Initial value
G07	Low SA	$1.17 \cdot 10^{-4}$	Initial value	97
G08		$7.68 \cdot 10^{-5}$	34	--
G09		$2.86 \cdot 10^{-4}$	63	--

TABLE 4 Relative increase/decrease of bulk resistivity depending on filler content (column 4) and on filler geometry ratio (column 5).

value ($5.14 \cdot 10^{-4}$ Ω cm). A further increment of 5.0 wt% in filler content has less effect, reducing the bulk resistivity by only $34\%_{rel}$. The opposite occurs when the bulk is mostly filled with LSA-fillers (green line). In this case, the initial increment in filler content (3.0 wt%) has a lower impact with a reduction of 34% relative to its initial value ($1.17 \cdot 10^{-4}$ Ω cm). A further increment of 3.0 wt% reduces the volume resistivity in $63\%_{rel}$. Following the same logical reasoning, a bulk that contains a similar amount of HSA and LSA fillers (red line) displays a balanced behavior when the filler content is increased – when the filler content is increased twice (4.0 wt% each time), the reduction in the bulk resistivity is 68% and 64% relative to its previous value.

The increase of LSA-fillers while reducing HSA-fillers at constant filler content has an opposite effect on the bulk resistivity. Each time that the filler geometry ratio is reduced (i.e., the relative proportion of LSA-filler is increased) while the total filler content is maintained, the bulk resistivity increases. Thus, the conductive LSA-fillers interrupt the better organized conductive matrix that the HSA-fillers can achieve by itself. For this situation it is rather difficult to isolate the source of a larger/smaller impact, as the first change in filler geometry ratio (*very high SA → high SA*) is done at 60 wt% while the second change (*high SA → medium SA*) is done at 70 wt%. Thus, there is a contribution due to the filler content at which the change in the filler geometry ratio was done. For example, the bulk resistivity decreases 167% when changing from group G00 to group G01, relative to group G00. In this case, the HSA-filler decreases 35% (100% → 65%), similarly, the HSA-filler decreases 34% (65% → 31%) when changing from group G03 to group G04. However, although this change is very similar (just 1% difference), the relative increase in the bulk resistivity is very different. In the second case the increase is $44\%_{rel}$ which may be different due to (a) the different total filler content at the point at which the filler geometry ratio is changed; (b) the initial value of the filler geometry ratio before it was reduced; (c) a synergy between both (a) and (b).

According to the percolation theory, the bulk resistivity (σ^{-1}) and the total filler content, φ, within the adhesive are related through the so-called *percolation threshold*, φ_c, with a power exponent known as the *universal exponent*, t. The normalized power exponent relationship is shown in **Equation (11)**, where 0 vol% and 100 vol% are 0 and 1.[11]

$$\sigma = \sigma_{Ag} \cdot \left(\frac{\varphi - \varphi_c}{1 - \varphi_c} \right)^t \qquad (11)$$

The value of t was believed to be universal and ranged between 1.6 and 2.0 for three-dimensional systems such as isotropic conductive adhesives.[11] Although this value is indeed mostly found in the universal range, it is sometimes found to be somewhat below or above this range when filler particles have extreme geometries. For instance, Carmona et al.[29] have obtained a value of t of 1.95 for carbon particles and a value as high as 3.1 for graphite particles in polymers. Deprez and McLachlan[30] obtained values of t in the range of 1.5–2.8 for a series of graphite (flaky) particles undergoing compaction. The percolation threshold is also known to be dependent on particle shape, the ratio of the filler and the matrix particle sizes, and interactions between the particles and the curing conditions for the adhesive.[11] Therefore, to a good approximation it is possible to correlate the resistivity of the adhesive and the silver content for each filler geometry ratio as:

$$y = \left(\frac{x - \varphi_c}{1 - \varphi_c} \right)^t \qquad (12)$$

where $y = \sigma \cdot (\sigma_{Ag})^{-1} = \rho_{Ag} \cdot (\rho)^{-1}$ and $x = \varphi$.

It is important to acknowledge that it is possible to use the percolation theory due to the following main reasons:

- The two fillers used for the different adhesive compositions are not extremely dissimilar nor possess extreme geometries when compared to each other.
- Both fillers are in the micrometer range; they are not nanoparticles.
- As both fillers are made of silver, the conductivity of the epoxy polymer is practically negligible in comparison.
- The total filler content range (60–84 wt%) that is investigated in this work is always above the percolation threshold. Therefore, the most suitable percolation theory equation is the one using the t exponent.

By fixing the exponent t to a particular value, φ_c can be determined by replacing the measured bulk resistivity shown in Table 4 with the respective filler content shown in Table 1 (column using vol %). The bulk resistivity of the silver particles, ρ_{Ag}, was assumed to be equal to $1.55 \cdot 10^{-6}$ (Ω cm).* The percolation threshold for each filler geometry ratio was determined as the average of the three results obtained using **Equation (12)** while maintaining the filler geometry ratio constant.

The graph shown in Figure 9 displays the average percolation threshold obtained for each filler geometry ratio when assuming different values of the exponent t plotted over the inverse of the filler geometry ratio (r^{-1}). As it can be seen, a second-grade polynomial fit better represents the data points than a linear fit. However, three points for a polynomial fit are too few to extrapolate this relationship to other filler geometry ratios. Therefore, the following analysis is only valid for the present dataset. As shown by the plot, the percolation threshold decreases with the inverse of the filler geometry ratio up to a certain point and then starts increasing. Hence, it is possible to find an optimum value of r that minimizes the percolation threshold. Assuming a polynomial fit $f(x) = ax^2 + bx + c$ and forcing its derivative to be zero ($0 = df(x)/dx = 2ax^* + b$), the optimum value of r^* ($1/x^*$) and its corresponding percolation threshold φ_c^* ($f(1/x^*)$) are determined and plotted in orange. The exact values are shown in Table 5.

The optimum percolation threshold tends to decrease ($1/r$ increases) for increasing values of the exponent t while simultaneously the adhesive requires more LSA-fillers to achieve this lower threshold. According to the data, the optimum percentage between HSA-fillers and LSA-fillers ranges between 38.66%–39.89% (HSA) and 60.11%–61.34%. By minimizing the percolation threshold, manufacturers are able to attain a certain electrical performance for an adhesive by using the minimum number of fillers required to achieve such capabilities. Thus, reducing the overall cost of manufacture without compromising performance.

4.3 | Contact resistivity of metallization–adhesive interface

It must be considered that for each composition at least 25 samples per group were manufactured to measure the contact resistivity. However, only the ones displaying a thin, straight, and homogeneous line were selected for electrical measurements. The number of samples per group varies from 8 up to 24, where the groups using an adhesive that is most viscous (higher filler content) tend to have a greater number of samples. The reason is simple: adhesives that are more viscous tend to spread less when external pressure is applied. Thus, the dispensed ECA line tends to be more consistent and homogeneous throughout its whole length.

As shown in Figure 10, the behavior of the contact resistance when increasing the total filler content and changing the filler geometry ratio is very similar to that of the bulk resistivity (compared with
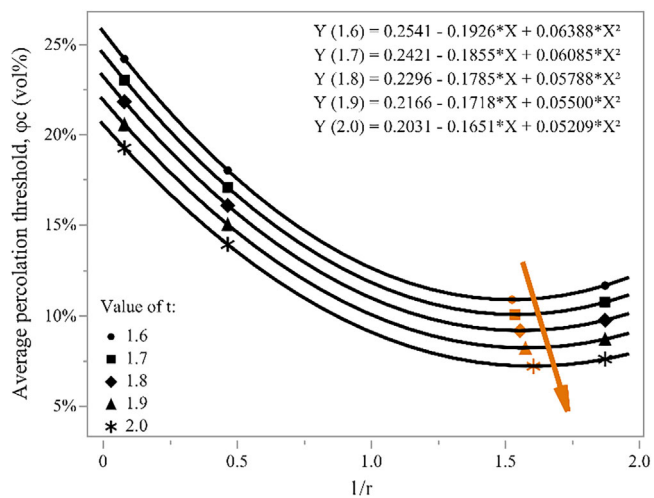
*Volume resistivity of 100% pure silver according to MatWeb Material Property Data.

FIGURE 9 Second-grade polynomial fit between average percolation threshold, φ_c, and the inverse of filler geometry ratio for different values of t. The minimum value of each fit, φ_c^*, is shown in orange with an arrow pointing to its trend.

TABLE 5 Optimum filler geometry ratio r that minimizes the percolation threshold, φ_c, for different values of t.

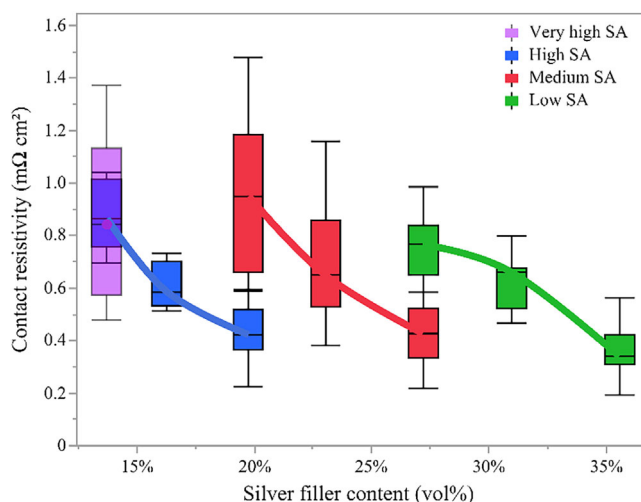| t	r^*	φ_c^*	Optimum HSA (%)	Optimum LSA (%)
1.60	0.6636	0.1090	39.89	60.11
1.70	0.6566	0.1008	39.64	60.36
1.80	0.6484	0.0919	39.33	60.67
1.90	0.6395	0.0823	39.01	60.99
2.00	0.6303	0.0722	38.66	61.34

FIGURE 10 Measured contact resistivity (in mΩ cm^2) for increasing total silver filler content.

Figure 8). However, the scale of the impact of the changes is not the same. As discussed in **Section 4.2**, the changes done to the adhesive induced up to an order of magnitude change in the bulk resistivity. In

contrast, the contact resistivity stays in the same order of magnitude no matter the changes. Table 6 shows the statistical metrics that are graphically displayed in Figure 10 and the calculated relative increase/decrease (in %) in the contact resistivity depending on what was changed (see columns 7 and 8 in Table 6).

According to Table 6 and Figure 10, the contact resistivity decreases with the increase in the filler content as expected. Depending on the filler geometry ratio, the impact in the reduction is different (see column 7). When the bulk contains a small amount of LSA-fillers (blue line) the initial increase in filler content (5.0 wt%, approx. 3 vol%) reduces the contact resistivity by 32% relative to its initial value (0.8642 mΩ cm^2). A further increment of 5.0 wt% has a smaller effect reducing the contact resistivity by only 28%$_{rel}$. The opposite occurs when the bulk is mostly filled with LSA-fillers (green line). In this case, the initial increment in filler content (3.0 wt%) has a lower impact with a reduction of 14% relative to its initial value (0.7653 mΩ cm^2), whereas a further increment of 3.0 wt% reduces the contact resistivity by 49%$_{rel}$. Similar to the previous case, for the medium surface area ratio (red line) an initial filler content increase of 4.0 wt% reduces the contact resistivity slightly less (32%$_{rel}$) than the second increment of 4.0 wt% (34%$_{rel}$).

According to Figure 10, there is a clear indication that for a certain filler content, there is a filler geometry ratio that minimizes the contact resistivity. More precisely, for a filler content of 19.6 vol%, a *high SA* filler geometry ratio is more beneficial (lower resistivity) than the *medium SA*, while for 27 vol%, a *medium SA* filler geometry ratio is more beneficial than the *low SA*. At 19.6 vol% the contact resistivity is 2.24 times larger at *medium SA* than at *high SA* filler geometry ratio. At 27 vol% the contact resistivity is 1.79 times larger for a *low SA* filler geometry ratio than at *medium SA*. Hence, the impact of the reduction of the contact resistivity when changing the filler geometry ratio is larger when the paste contains more HSA-fillers.

Table 6 shows that σ_{G00} and Σ_{G00} are the highest. Additionally, the box and whisker plot in Figure 10 indicates a slight skewness to lower values. Due to this reason, it may be possible that the most accurate value of $\rho_{c,G00}$ is indeed smaller than $\rho_{c,G01}$. Nevertheless, the

values should not be that different. This means that the impact on the contact resistivity when changing the filler geometry ratio from *very high SA* to *high SA* is very small (2.7%$_{rel}$). Similar to the volume resistivity, the highest impact in the contact resistivity is due to a change from *high SA* to *medium SA* (125%$_{rel}$). This may be due to an inflection point, where the adhesive changes from having more HSA-fillers (65%) than LSA-fillers (35%) to having more LSA-fillers (69%) than HSA-fillers (31%). After that, any increment of LSA-fillers seems to have a lower effect with a contact resistivity increment of 79%$_{rel}$ when changing from *medium SA* to *low SA*.

4.4 | Relationship between bulk and contact resistivity

Although bulk and contact resistivity behave similarly when the filler content is increased and the filler geometry ratio changes, the degree of impact is considerably different. Figure 11 shows the relation
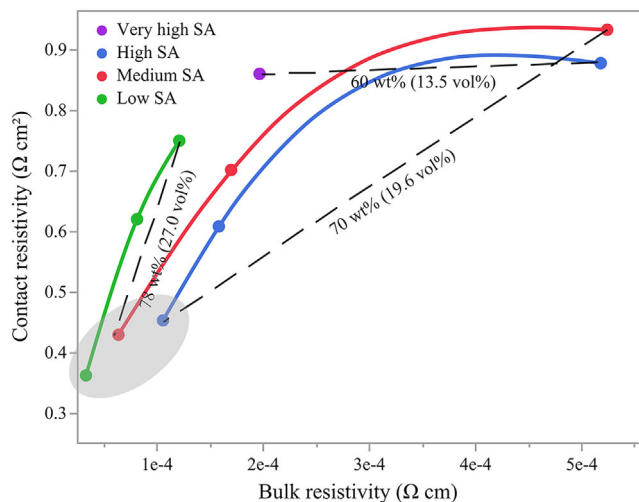

FIGURE 11 Contact vs. bulk resistivity for all filler geometry ratios under study.

TABLE 6 Statistical metrics for the contact resistivity for groups G00 – G09, where ρ_c is the median, σ, and Σ are the absolute and relative deviation of the median and *n* is the number of samples. The table includes the relative increase/decrease of contact resistivity depending on filler content (column 7) and on filler geometry ratio (column 8).

Group	Filler geometry ratio	ρ_c (mΩ cm^2)	σ (mΩ cm^2)	Σ (%)	n	$|\Delta\%_{rel}|$	
G00	Very high SA	0.8415	0.2774	32.96	12	--	Initial value
G01	High SA	0.8642	0.1199	13.87	8	Initial value	2.7
G02		0.5858	0.0706	12.06	12	32	--
G03		0.4221	0.0709	16.79	17	28	Initial value
G04	Medium SA	0.9494	0.2631	27.72	9	Initial value	125
G05		0.6482	0.1393	21.48	16	32	--
G06		0.4270	0.0919	21.51	24	34	Initial value
G07	Low SA	0.7653	0.0933	12.20	12	Initial value	79
G08		0.6610	0.0567	8.57	21	14	--
G09		0.3404	0.0400	11.76	20	49	--

between contact (y-axis) and bulk (x-axis) resistivities for all the different filler geometry ratios under study. The dashed lines indicate changes in filler geometry ratio for a fixed filler content. At 60 wt% when the filler geometry ratio changes from *very high SA* to *high SA*, the bulk resistivity is nearly doubled while the contact resistivity is practically constant or increases negligibly in comparison. In contrast, the opposite happens when the adhesive is filled with 78 wt% and the ratio changes from *medium SA* to *low SA*. In this second case, the bulk resistivity changes negligibly when compared to the contact resistivity, which is nearly doubled. Importantly, Figure 11 shows that the filler content can be reduced from 84 wt% to 70 wt% with only minimal increases in bulk and contact resistivities (shaded region, bottom left).

The main advantage of an HSA-filler is to reduce bulk resistivity by (1) diminishing the constriction resistance between the fillers that are directly in contact and (2) by allowing electrons to travel greater distances through the bulk of a filler instead of the insulating matrix; it is believed that by increasing the percentage of the LSA-fillers, percolation paths are disrupted by the new filler geometry. The probable reason is that the substitution of a thin extended HSA-filler by the same volume fraction of a compact LSA-filler results in an accumulation of conductive metal. At the percolation threshold, it is reasonable that accumulation reduces the formation of percolation clusters (see

Figure 1). This impact may be larger in the bulk than at the contacting interface between ECA and metallization due to two main factors. Two formulations containing the lowest filler content (60 wt%) show a large impact on bulk resistivity by substitution of HSA-fillers. At the percolation threshold HSA-fillers may result in a higher probability of in-bulk contact between extended filler particles due to higher spatial distribution than agglomerated compact LSA-filler particles (see the difference between fillers in Figure 2). Figure 12 shows a cross-section at two different positions of the adhesive from group G00 (*very high SA*) while Figure 13 shows the same information but of the adhesive from group G01 (*high SA*). Both ECAs show at the cross-section a comparable Ag-filler fraction of around 36 vol%. It seems likely that the space between the fillers is increased when the LSA-fillers are introduced (Figure 12 → Figure 13).

In contrast, the green line in Figure 11 shows that the effects at higher total Ag-filler content are inverted. At a filler content of 78 wt % there are a larger number of particles within the bulk. Hence, even if the percentage of LSA-filler is greatly increased, the packing density and redundancy (by multi-bonds) in the direct contact of fillers is so high that the LSA-filler shape cannot disrupt single- and multi-bonds to such a large degree as it does it at 60 wt%. Figure 14 shows a SEM cross-section of the bulk of the ECA from group G06 (*medium SA*)
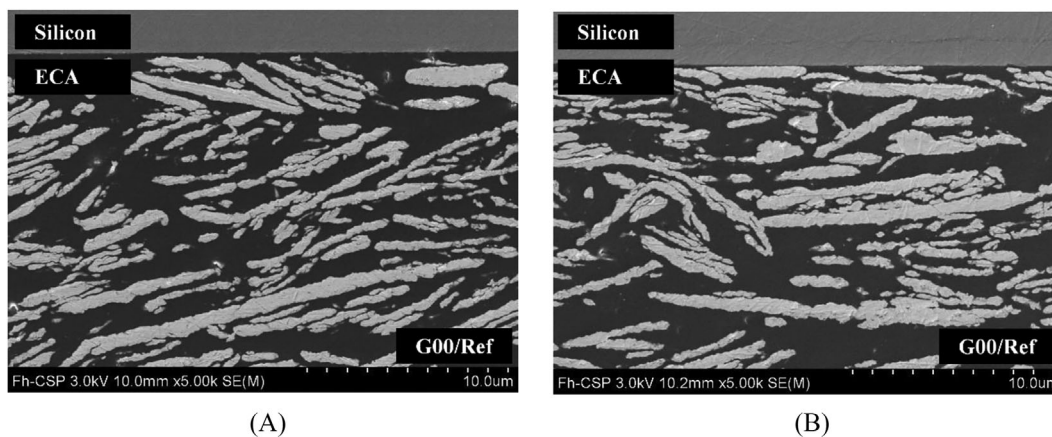

(A) (B)

FIGURE 12 SEM cross-section at two different positions 8 mm apart within the same sample using ECA G00 (*very high SA*).
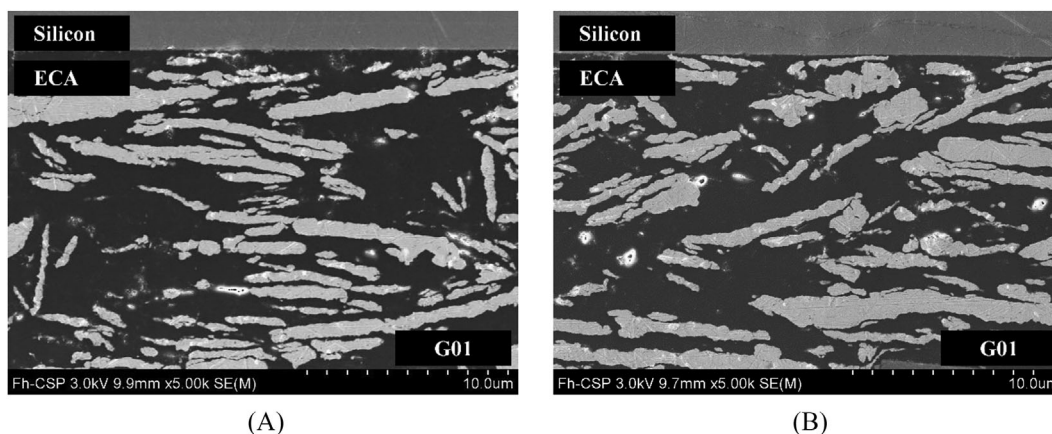

(A) (B)

FIGURE 13 SEM cross-section at two different positions 8 mm apart within the same sample using ECA G01.

while Figure 15 shows that from group G07 (*low SA*). Both ECAs show at the cross-section a comparable Ag-filler fraction of around 46 vol%. As shown in these two SEM images, G07 with a dominant *low SA* filler fraction does not exhibit extended fillers compared to G06. LSA particles are clearly bulkier in group G07 but did not affect the bulk resistivity as explained before.

The true impact of the filler shape on the contact resistance is more complicated and cannot be concluded by the performed measurements. Nevertheless, a hypothesis could be as follows. In contrast to within the bulk, at the interface, one half-space of the contact consists of a conductive material (the metallization paste). In the other half-space (the ECA), every Ag-filler at the interface would establish contact with the conductive material. SEM images shown in Figure 12 also reveal that HSA-fillers tend to lay within the ECA bulk parallel to the wafer surface. This is believed to be influenced by the preparation of the adhesive and the mechanical pressure that is applied during the curing process. This means that at a *medium SA* filler geometry ratio, up
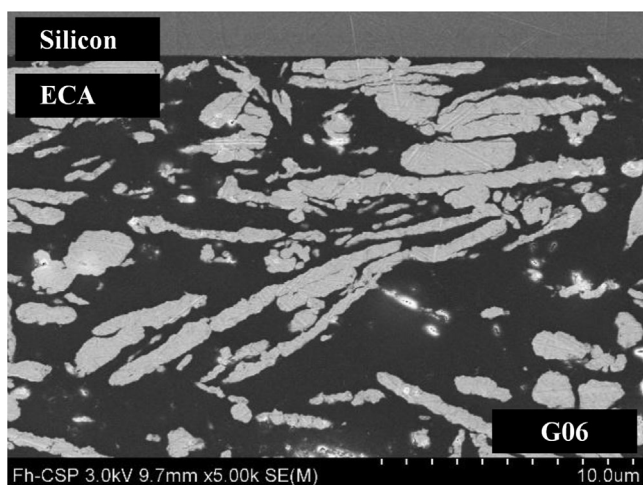

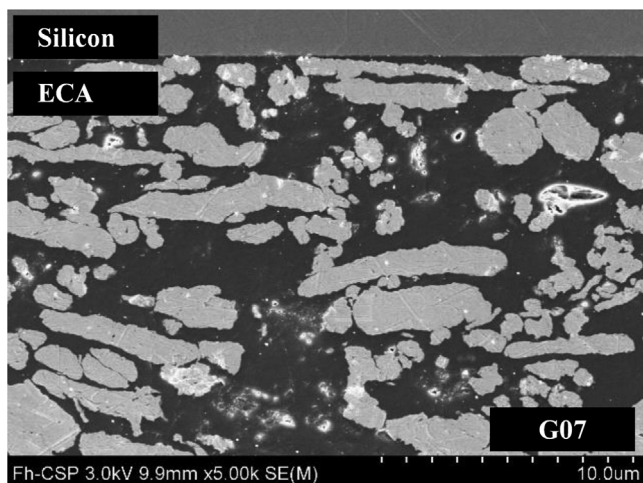**FIGURE 14**   SEM cross-section of the bulk using ECA from group G06 (*medium SA*).

FIGURE 15   SEM cross-section of the bulk using ECA from group G07 (*low SA*).

to 30% of the contacting interface could be formed by HSA-fillers laying parallel to the metallization paste. Due to the high surface area, it could be that large area contact formation is enhanced for the HSA-fillers. If so, reducing the percentage of HSA-fillers to 6% would replace large contacting areas between the HSA-fillers and the metallization paste with several smaller contacting points. Since the packing density is higher, such a reduction would have a greater impact on the contact resistivity. Nevertheless, the given hypothesis cannot be conclusively deduced from the SEM measurements and further proof would be needed to validate this hypothesis versus alternative explanations.

5 | CONCLUSIONS

This work shows the impact of the increase in filler content on the bulk resistivity of an epoxy-based conductive adhesive and the contact resistivity between the adhesive and a metallization paste used on solar cells. Both adhesive and metallization pastes use silver particles. To control the viscosity and processability of the conductive adhesive when the total filler content is increased, two different fillers were used consisting of high or low surface area (HSA and LSA) particle geometry. Thus, the impact of changing the ratio of filler geometries (i.e., filler geometry ratio LSA/HSA) was also analyzed. As expected, it was found that the contact and bulk resistivities decreased when the filler content was increased. However, the magnitude of the decrease was found to depend strongly on the filler geometry ratio.

At extreme filler geometry ratios, when the bulk is either mostly loaded with HSA-fillers or mostly with LSA-fillers, the impact of changes in the filler content on the bulk and contact resistivities is markedly different. Particularly, at a low filler content (60 wt%), changing the filler geometry ratio can lead to a doubling of the bulk resistivity while the contact resistivity is relatively unaffected. In contrast, at a high filler content (78 wt%), changing the filler geometry ratio can lead to a doubling of the contact resistivity while the bulk resistivity is relatively unchanged. The measured data was interpreted within the context of percolation theory and it was determined that the optimum ratio of the LSA and HSA fillers investigated in this study is approximately 60:40. Hence, the contact formation (bulk and interface) near the percolation threshold can be tuned by careful design of filler geometry properties and compositions. Nevertheless, further microstructure analysis is needed to reveal evidence of the percolation structure tuning by filler geometry for filler contents near this threshold, where single bonds between percolation clusters become dominant.

This work has important ramifications for the design of ECAs, where cost considerations and the need to reduce silver resource usage demand the lowest (silver) filler content, but the demands of product performance point to higher filler content. In particular, this work clearly shows that by optimizing mixtures of different particle geometries, it is possible to significantly reduce the silver content of ECAs with only minimal increase in bulk and contact resistivity. The use of different particles and mixtures of particle geometries can thus be expected to allow even further decreases in filler content without significant loss of ECA performance.

DATA AVAILABILITY STATEMENT

Research data are not shared.

ORCID

Maria Ignacia Devoto Acevedo https://orcid.org/0000-0002-2393-1225

Ralph Gottschalg https://orcid.org/0000-0002-0066-0899

Daniel Tune https://orcid.org/0000-0002-8330-555X

REFERENCES

1. Devoto Acevedo MI, Wienands K, Timofte T, Halm A, Gottschalg R, Tune D. Influence of micro– and macrostructure when determining the contact resistivity of interconnects based on electrically conductive adhesives. *Solar Energy Mater Solar Cells*. 2023;260:112490. doi:10.1016/j.solmat.2023.112490

2. McLachlan DS. Evaluating the microstructure of conductor-insulator composites using effective media and percolation theories. *MRS Proc*. 1995;411:309. doi:10.1557/PROC-411-309

3. Habenicht G. *Kleben: Grundlagen, Technologien, Anwendungen*. Springer Berlin Heidelberg; 2009. doi:10.1007/978-3-540-85266-7

4. Wu J, McLachlan DS. Percolation exponents and thresholds obtained from the nearly ideal continuum percolation system graphite-boron nitride. *Phys Rev B*. 1997;56(3):1236-1248. doi:10.1103/PhysRevB.56.1236

5. Li L, Morris JE. Electrical conduction models for isotropically conductive adhesives. *J Electron Manuf*. 1995;05(04):289-296. doi:10.1142/S096031319500030X

6. Clingerman ML, King JA, Schulz KH, Meyers JD. Evaluation of electrical conductivity models for conductive polymer composites. *J Appl Polym Sci*. 2002;83(6):1341-1356. doi:10.1002/app.10014

7. Li L, Morris JE. Electrical conduction models for isotropically conductive adhesive joints. *IEEE Trans Comp Pack Manuf Technol: Part A*. 1997;20(1):3-8. doi:10.1109/95.558537

8. Mohd Radzuan NA, Sulong AB, Sahari J. A review of electrical conductivity models for conductive polymer composite. *Int J Hydrogen Energy*. 2017;42(14):9262-9273. doi:10.1016/j.ijhydene.2016.03.045

9. Lux F. Models proposed to explain the electrical conductivity of mixtures made of conductive and insulating materials. *J Mater Sci*. 1993;28(2):285-301. doi:10.1007/BF00357799

10. McLachlan DS. Measurement and analysis of a model dual conductivity medium using a generalized effective medium theory. *Phys a: Stat Mech Appl*. 1989;157(1):188-191. doi:10.1016/0378-4371(89)90299-9

11. McLachlan DS, Blaszkiewicz M, Newnham RE. Electrical resistivity of composites. *J am Ceram Soc*. 1990;73(8):2187-2203. doi:10.1111/j.1151-2916.1990.tb07576.x

12. Mamunya EP, Davidenko VV, Lebedev EV. Effect of polymer-filler interface interactions on percolation conductivity of thermoplastics filled with carbon black. *Compos Interfaces*. 1996;4(4):169-176. doi:10.1163/156855497X00145

13. Malliaris A, Turner DT. Influence of particle size on the electrical resistivity of compacted mixtures of polymeric and metallic powders. *J Appl Phys*. 1971;42(2):614-618. doi:10.1063/1.1660071

14. Nielsen LE. The thermal and electrical conductivity of two-phase systems. *Ind Eng Chem Fund*. 1974;13(1):17-20. doi:10.1021/i160049a004

15. Bigg Battelle DM. Conductive polymeric compositions. *Polym Eng Sci*. 1977;17(12):842-847. doi:10.1002/pen.760171206

16. Weber M, Kamal MR. Estimation of the volume resistivity of electrically conductive composites. *Polym Compos*. 1997;18(6):711-725. doi:10.1002/pc.10324

17. Zallen R. *The physics of amorphous solids*. Wiley; 1998. doi:10.1002/9783527617968

18. Bergman DJ, Stroud D. Physical properties of macroscopically inhomogeneous media. *Solid State Phys - Adv Res Appl*. 1992;46(C):147-269. doi:10.1016/S0081-1947(08)60398-7

19. Nan C-W. Physics of inhomogeneous inorganic materials. *Prog Mater Sci*. 1993;37(1):1-116. doi:10.1016/0079-6425(93)90004-5

20. McLachlan DS, Rosenbaum R, Albers A, et al. The temperature and volume fraction dependence of the resistivity of granular Al-Ge near the percolation threshold. *J Phys Condens Matter*. 1993;5(27):4829-4842. doi:10.1088/0953-8984/5/27/027

21. Pike GE. Conductivity of thick film (cermet) resistors as a function of metallic particle volume fraction, in *AIP Conference Proceedings*, AIP, 1978; 366–371. 10.1063/1.31163.

22. Carmona F, Prudhon P, Barreau F. Percolation in short fibres epoxy resin composites: conductivity behavior and finite size effects near threshold. *Solid State Commun*. 1984;51(4):255-257. doi:10.1016/0038-1098(84)91008-1

23. Lee S-I, Song Y, Noh TW, Chen X-D, Gaines JR. Experimental observation of nonuniversal behavior of the conductivity exponent for three-dimensional continuum percolation systems. *Phys Rev B*. 1986;34(10):6719-6724. doi:10.1103/PhysRevB.34.6719

24. Sandler JKW, Kirk JE, Kinloch IA, Shaffer MSP, Windle AH. Ultra-low electrical percolation threshold in carbon-nanotube-epoxy composites. *Polymer (Guildf)*. 2003;44(19):5893-5899. doi:10.1016/S0032-3861(03)00539-1

25. Mutlay I, Tudoran LB. Percolation behavior of electrically conductive graphene nanoplatelets/polymer nanocomposites: theory and experiment. *Fullerenes Nanotubes Carbon Nanostruct*. 2014;22(5):413-433. doi:10.1080/1536383X.2012.684186

26. Agarwal M, Sharma S, Shankar V, Joshi YM. Distinguishing thixotropy from viscoelasticity. *J Rheol (N Y N Y)*. 2021;65(4):663-680. doi:10.1122/8.0000262

27. Durairaj R, Ekere NN, Salam B. Thixotropy flow behaviour of solder and conductive adhesive pastes. *J Mater Sci Mater Electron*. 2004;15(10):677-683. doi:10.1023/B:JMSE.0000038923.62923.1e

28. Devoto Acevedo MI, Wienands K, Rudolph D, et al. Validation of methodology to determine the contact resistivity of ECA-based bonds grounded on end–contact resistance measurements using redundant and modified TLM test structures. *Solar Energy Mater Solar Cells*. 2023;262:112518. doi:10.1016/j.solmat.2023.112518

29. Carmona F, Canet R, Delhaes P. Piezoresistivity of heterogeneous solids. *J Appl Phys*. 1987;61(7):2550-2557. doi:10.1063/1.337932

30. Deprez N, McLachlan DS. The analysis of the electrical conductivity of graphite conductivity of graphite powders during compaction. *J Phys D Appl Phys*. 1988;21(1):101-107. doi:10.1088/0022-3727/21/1/015